Available online at www.sciencedirect.com

ScienceDirect

Transportation Research Procedia 70 (2023) 91–98

Transportation Research Procedia

www.elsevier.com/locate/procedia

8th International Electric Vehicle Conference (EVC 2023)

Experimental Investigation of Voltage Limitation Modes and State of Power Estimation for a High-Power Lithium-Ion Battery

Adriano Schommer[a,*], Marcelo A. Xavier[b], Denise Morrey[a], Gordana Collier[a]

[a]*Oxford Brookes University, Wheatley Campus, Oxford, OX33 1HX, UK.*
[b]*Project Kuiper, Amazon, Inc. Redmond, WA, USA.*

Abstract

This paper investigates the behaviour of a high-power lithium-ion battery (LIB) pouch cell under voltage limitation at a high state of charge (SOC). The state of power (SOP) estimation is crucial in providing insights into optimising energy recovery during regenerative braking events. Experiments were conducted at different high-charging C-rates to analyse the voltage limitation modes and to assess the accuracy of a model-based SOP estimation algorithm developed based on published literature. The results show that the accuracy of the battery model alone is not sufficient to address the accuracy of the SOP estimation algorithm. Furthermore, different voltage limitation modes are discussed and the average power output is investigated. For example, it was observed that Constant-Current Constant-Voltage (CCCV) mode outputs 59.75% more power than Constant-Current (CC) pulses. These findings provide valuable insights into the behaviour of high-power LIB pouch cells and offer a foundation for further research to improve regenerative braking performance for motorsport applications.

Keywords: State of Power estimation; peak power; available power; lithium-ion; CCCV; CC.

1. Introduction

Lithium-ion batteries have specific voltage, current, and temperature operating limits which are defined by the manufacturer. As a result, a battery management system (BMS) is required to regulate the operation of a battery pack, mitigating rapid ageing and preventing safety risks. The BMS act as both a control and predictive system. The control system focuses on cell balancing and safety-critical aspects, such as contactor control and fault management, while the predictive system uses algorithms to estimate internal battery states to optimise performance and extend battery life. Among the predictive algorithms, the state of power (SOP) estimation is responsible for computing power limits of the battery for a given time window, with the goal of enhancing performance while acting as a safety boundary for the battery pack (Yang et al., 2020).

* Corresponding author. adriano.schommer@brookes.ac.uk
E-mail address: adriano.schommer@brookes.ac.uk

2352-1465
10.1016/j.trpro.2023.11.006

In automotive applications, vehicle performance is limited by multiple hardware constraints that are a function of environmental conditions – e.g. temperature and humidity; drive cycle specific conditions – e.g. highway, city; and driving style. The SOP estimation is one of these limiting layers, providing information to the vehicle control unit (VCU) to make better-informed decisions on when and how to limit power. In motorsport applications, the state of power is essential for optimising energy recovery during braking events (regenerative braking). At a high state of charge (SOC), regenerative braking is limited by the battery pack's ability to absorb the energy, specifically by the upper voltage limit of the cells.

This paper investigates the behaviour of a high-power LIB pouch cell under voltage limitation at high SOC (> 0.98). Experiments were performed at different high-charge C-rates, providing insights into the voltage limiting modes and providing validation data for the SOP estimation algorithm developed based on (Plett, 2015b). More specifically, Constant-Current Constant-Voltage (CCCV) and Constant-Current (CC) pulses were compared for power output. The experimental findings of this paper support the argument that the CC pulse does not utilise the cell's full potential (Esfandyari et al., 2019; Pei et al., 2014).

The organisation of this paper is as follows: Section 2 gives an overview about SOP estimation, defines the problem being addressed and explores the model-based algorithm used in this research. Section 3 addresses the experimental setup and the verification tests. Results are presented in Section 4, comparing the experimental investigation to the algorithm prediction. Finally, results are discussed in section 5, and this paper is concluded in section 6.

2. State of Power estimation

2.1. Problem definition

State of power estimates the maximum power available over the next Δt seconds, herein referred to as the future horizon. Because power at a discrete time step, k is defined as a function of the terminal voltage v and current i (Equation 1), it is convenient to frame the problem in terms of voltage and current.

$$P[k] = v[k]\, i[k] \tag{1}$$

Cell manufacturers commonly define design limits in terms of current, voltage, SOC and temperature. That leads to several possible combinations of limits, for example, the current that will lead the cell to reach maximum temperature $\left(i_{max}^{temp}\right)$, state of charge $\left(i_{max}^{SOC}\right)$ or voltage $\left(i_{max}^{volt}\right)$. Therefore, the state of power of a battery is defined as the most limiting current among all these combinations, defined as in Equation 2 for charge:

$$i_{max}^{chg} = max\left(i_{max}^{chg,C_{rate}}, i_{max}^{chg,SOC}, i_{max}^{chg,volt}, i_{max}^{chg,temp}\right) \tag{2}$$

Fig. 1a illustrates the future horizon, where the SOP algorithm searches for the current that will cause the cell to reach any design limits over the future horizon, and Fig. 1b further explores the three possible limiting modes:

I. Constant-Voltage (CV). The terminal voltage is clamped at v_{lim} during the entire horizon Δt. Consequently, the current varies by decreasing at each time step as a function of the terminal voltage. Therefore $i_{max}^{chg,volt}[k] > i_{max}^{chg,volt}[k + k_{\Delta t}]$, where $k_{\Delta t}$ is the time step at the end of the future horizon Δt.

II. Constant-Current (CC). A constant current $i_{max}^{chg,volt}$ causes the cell to reach the maximum voltage limit, usually, at the end of the future horizon so that $v[k + k_{\Delta t}] = v_{max}$. Therefore, $i_{max}^{chg,volt}[k] = i_{max}^{chg,volt}[k + k_{\Delta t}]$.

III. Constant-Current Constant-Voltage (CCCV). The cell is first limited by a constant current $i[k] = i_{max}^{chg,volt}$ similar to the limit mode II, followed by the constant voltage limit of mode I. Therefore, $i_{max}^{chg,volt}[k] > i_{max}^{chg,volt}[k + k_{\Delta t}]$.

From the three limiting modes, only limit mode II (CC) can be expressed as a single value because the current is constant. For this case, the SOP during charge is defined as in Equation 3, for which the SOP algorithm searches for the i_{max}^{chg}. This paper focuses on the charge voltage limit at high SOC using CC pulses.

$$P_{max}^{chg}[k + k_{\Delta t}] = v_{max}[k + k_{\Delta t}]\, i_{max}^{chg} \tag{3}$$

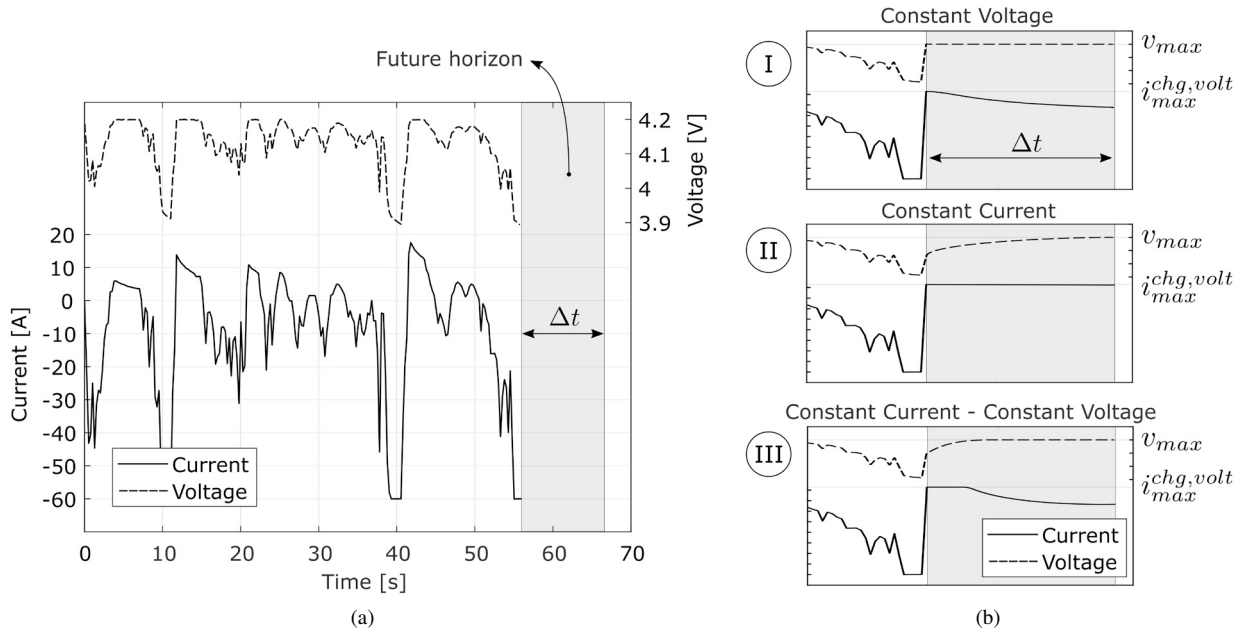

(a) (b)

Fig. 1: a) Respecting multiple design constraints, the SOP algorithm estimates the maximum power available over a future horizon Δt. b) A cell under charging load can be voltage limited in three different modes: I – Constant Voltage (CV) mode, II – Constant Current (CC) mode, III – combined Constant Current Constant Voltage (CCCV) mode. Here, v_{max} represents the maximum operating voltage, and $i_{max}^{chg,volt}$ denotes the maximum current that causes the cell to reach the voltage limit.

2.2. Battery model

The experiments described in this paper made use of an Equivalent Circuit Model (ECM) comprised by a SOC and temperature dependent voltage source, a series resistance and a single resistor-capacitor pair, as depicted in Fig. 2. The resistor element models the ohmic resistance, responsible for the fast dynamics of the cell (instantaneous polarization), while the *RC* network model the slower polarization effects.

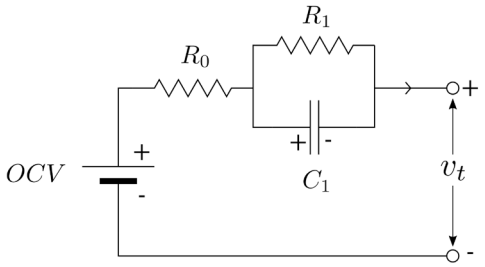

Fig. 2: Single *RC* Equivalent Circuit Model (Thevenin Model).

In this model, *OCV* is a SOC and temperature dependent voltage source, R_0 is the ohmic resistance, R_1 and C_1 are the charge-transfer resistance and the double-layer capacitance of the *RC* network. More specifically, R_1 models the resistance of the electrode-electrolyte interface, and C_1 models the electrolyte charge build up at the electrode surface (Plett, 2015a). The equations of this model are better described in discrete-time state-space form as follows:

$$x[k+1] = \boldsymbol{A}x[k] + \boldsymbol{B}u[k] \tag{4}$$

$$y[k] = \boldsymbol{C}x[k] + \boldsymbol{D}u[k] \tag{5}$$

Equation 4 is the input equation, where x is the state vector and u is the input vector. $\boldsymbol{A}$ and $\boldsymbol{B}$ are the state and the input matrices, respectively. Equation 5 is the output equation, where y is the output vector, function of the state and input vectors, the output matrix $\boldsymbol{C}$, and the feed-through matrix $\boldsymbol{D}$. In these equations, the present time instant is denoted as $[k]$ and the updated time instant as $[k+1]$. In continuous form, the discrete time instants would be equivalent to $t_0 = k\Delta t$ and $t_0 = (k+1)\Delta t$, where Δt is the sample time at which a microcontroller processes the data.

For convenience, the state vector was designed in this paper to include the current through the resistance element of the RC pair i_{R1} and the state of charge z, which results in Equations 6 and 7:

$$\begin{bmatrix} z\,[k+1] \\ i_{R_1}\,[k+1] \end{bmatrix} = \begin{bmatrix} 1 & 0 \\ 0 & \exp\left(\frac{-\Delta t}{R_1 C_1}\right) \end{bmatrix} \begin{bmatrix} z\,[k] \\ i_{R_1}\,[k] \end{bmatrix} + \begin{bmatrix} \frac{\eta[k]\Delta t}{Q} \\ 1 - \exp\left(\frac{-\Delta t}{R_1 C_1}\right) \end{bmatrix} i\,[k] \tag{6}$$

$$v\,[k] - OCV\,[k] = R_1 i_{R_1}\,[k] + R_0 i\,[k] \tag{7}$$

where, $v\,[k]$ is the terminal voltage, $OCV[k]$ is the open circuit voltage, $i\,[k]$ is the current demand, and $\eta[k]$ is the coulombic efficiency.

In this paper, the open-circuit voltage was approximated by pseudo-OCV tests, and the circuit parameters were estimated using HPPC tests. The data used for the ECM characterisation comes from the open-source Oxford Brookes Battery Test Consortium (Planden et al., 2021). For enhanced accuracy, the parameters were estimated as a function of temperature and SOC, and further calibrated using the dynamic data shown in Fig. 1a.

2.2.1. Voltage limit

For a given future horizon Δt, the SOP algorithm computes the absolute maximum constant current that the battery can sustain such that the terminal voltage does not exceed the design limits v_{min} and v_{max}. The algorithm uses the 1-RC ECM to predict the future voltage $v\,[k + k_{\Delta T}]$ at the end of the future horizon $Fig.\Delta t$. The ECM works in combination with a search algorithm that finds the constant current $i\,[k]$ that satisfies the cost function in Equation 8. That is, when $i\,[k] = i_{min,k}^{chg,volt}$.

$$0 = v\,[k + k_{\Delta T}] - v_{max} \tag{8}$$

The future voltage prediction is calculated as in Equation 9:

$$v\,[k + k_{\Delta T}] = OCV\,[k + k_{\Delta T}] + R_1 i_{R_1}\,[k + k_{\Delta T}] + R_0 i\,[k] \tag{9}$$

The term $i_{R_1}\,[k + k_{\Delta T}]$, can be calculated using Equation 6 for a number of time steps k so that $k_{\Delta t} = \Delta T$. Alternatively, Plett (2015b) presents an efficient approach that calculates the i_{R_1} directly at $[k + k_{\Delta T}]$. It takes advantage of the special case where the state equation is linear – when the input current $i\,[k]$ and the ECM parameters R_0, R_1 and C_1 are constant over the future horizon Δt. For a complete derivation of the equations, the reader is referred to (Plett, 2015b). Here, only the final steps of the derivation are presented:

$$x\,[k + k_{\Delta T}] = \boldsymbol{A}^{k_{\Delta T}} x\,[k] + \left(\sum_{j=0}^{k_{\Delta T}-1} \boldsymbol{A}^{k_{\Delta T}-1-j} \right) \boldsymbol{B} u\,[k] \tag{10}$$

where, $\sum_{j=0}^{k_{\Delta T}-1} \boldsymbol{A}^{k_{\Delta T}-1-j} = \begin{cases} (\boldsymbol{A} - \boldsymbol{I})^{-1} \left(\boldsymbol{A}^{k_{\Delta T}} - \boldsymbol{I} \right) & \text{for elements} < 1 \\ k_{\Delta T} & \text{for elements} = 1 \end{cases}$ which, for the $i_{R_1}\,[k + k_{\Delta T}]$ term, leads to:

$$i_{R_1}\,[k + k_{\Delta T}] = \exp\left(\frac{-\Delta t}{R_1 C_1}\right)^{k_{\Delta T}} i_{R1}\,[k] + \left(\frac{1 - \exp\left(\frac{-\Delta t}{R_1 C_1}\right)^{k_{\Delta T}}}{1 - \exp\left(\frac{-\Delta t}{R_1 C_1}\right)} \right) \left(1 - \exp\left(\frac{-\Delta t}{R_1 C_1}\right) \right) i\,[k] \tag{11}$$

Finally, the bisection root finding algorithm is applied with Equations 8 and 9 to search for the maximum current that can be applied respecting the voltage hard constraints defined by the cell manufacturer. A detailed description of the bisection algorithm can be found in (Plett, 2004).

3. Experimental setup

The experimental setup of the tests consisted of an Arbin LBT-21084-HC cell cycler connected to a single 6.8 Ah Melasta SLPBB142124 Lithium Cobalt Oxide (LCO) pouch cell. The upper limit voltage of the cell is 4.2V and the maximum C-rate is 4. The test schedule, controlled by a host computer, included charge CC, CCCV pulses and a load profile based on the track layout of a Formula Student endurance event. The drive cycle shown in Fig.1a is one lap of the 22 laps of the endurance event and was developed by the 2023 Oxford Brookes Racing (OBR) Formula Student team using the AVL VSM™ software. The drive cycle represents the performance of the OBR 2023 Formula Student vehicle. The ambient temperature was controlled by a Binder KB115 thermal chamber set to 25°C. To be representative of the mechanical constraints of the cell when assembled in the battery pack, the pouch cell was tested using a constant displacement fixture developed by (Lukow, 2021) with the initial face pressure set to zero.

3.1. Verification tests

3.1.1. Constant-Current (CC)

Finding the maximum current, $i_{max}^{chg,volt}$ experimentally is an iterative process. Incremental constant current pulses are performed until the voltage limit is reached at the end of the future horizon. This paper took advantage of the method proposed by (Guo and Shen, 2022) to reduce the number of test attempts. Data from three different current pulses were used to calculate the theoretical limit by fitting a linear equation to the data. The tests performed by Guo allowed the cell sufficient relaxation time to reach equilibrium before the pulses were performed – the so-called static SOP tests. In this paper, we assessed if the method would still work under dynamic conditions (with no relaxation before the pulses) to further decrease testing time. Therefore, four CC pulses of 10 seconds were performed (Fig. 3a) at the end of the endurance drive cycle (Fig. 3b), resulting in:

$$i_{max}^{chg,volt} = 179.955 v_{max} - 747.67 \tag{12}$$

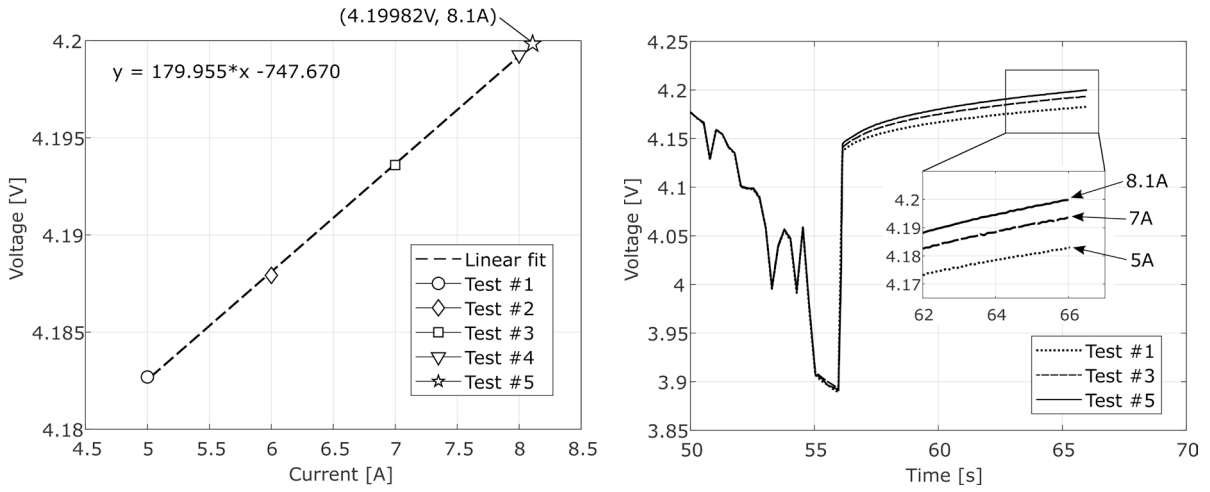

Fig. 3: Constant Current pulse tests to find $i_{max}^{chg,volt}$ a) A linear equation was fitted into four CC pulses (tests #1 to 4) to find the theoretical maximum current. Based on the calculations, the 8.1A CC test #5 was performed, reaching 4.19982V. b) Voltage profile of CC tests. For enhanced clarity, only tests #1, #3 and #5 are shown.

Using the Equation 12, The theoretical calculation for $i_{max}^{chg,volt}$ was 8.141A, whilst test #5 was performed with 8.1A. No further attempts were made because the difference between the theoretical (desired) and measured voltage was $< 0.05mV$ which was considered within the experimental error of the test.

3.1.2. Constant Current Constant Voltage (CCCV)

In addition to the CC tests, a CCCV test was performed to assess the difference in power output between the limiting modes. The same Formula Student drive cycle was used but with CCCV pulses clamping the voltage at $v_{max} = 4.2V$.

4. Results

The accuracy of the SOP estimation algorithm employed in this paper is limited by the accuracy of the ECM it relies upon. Thus, it is considered good practice to present the accuracy of the ECM. Fig. 4a shows the error of the model for a single lap of the Formula Student drive cycle followed by the 10 seconds CC pulse. A Root Mean Squared Error (RMSE) = 2.321mV and a Mean Absolute Error = 1.713mV were found. The maximum absolute error was 8.357mV.

Fig. 4b presents the maximum current estimated by the bisection algorithm compared to the experimental results. Additionally, it displays the load profile used prior to the CC pulse. It is important to note that the intersection between the bisection algorithm estimation and the load profile does not imply that the load profile exceeds the current limits set by the algorithm. This distinction arises because the algorithm estimates the current limit for a future horizon of 10 seconds, rather than considering instantaneous power availability. Hence, direct comparisons of the validation experiments should be limited to the future horizon highlighted by the grey area, where a CC pulse of 10s is applied.

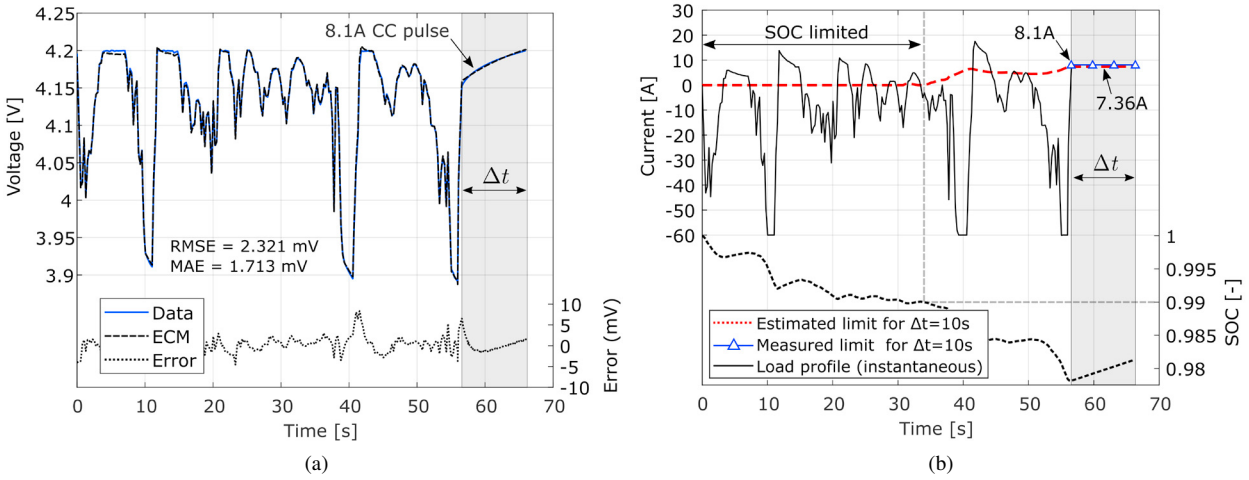

Fig. 4: State of power estimation results for a future horizon $\Delta t = 10s$. a) ECM results. b) Bisection algorithm results.

In Fig. 4b, an upper hard constraint of SOC= 0.99 was arbitrarily included to assess the behavior of the algorithm, demonstrated in the first 35 seconds of the load profile. The maximum allowed current is zero because the cell is operating at SOCs above 0.99. From 35s to 57s the bisection algorithm predicts the maximum available power for a CC pulse of 10s. The estimated i_{max}^{chg} is 7.36A whilst the measured limit is 8.1A, a difference of 10%.

Fig. 5 presents the experimental results of CCCV and CC charge pulses for 10s. This test quantifies the cell's power output operating at peak power under the CCCV and CC voltage limit. 5a shows the voltage and current profiles, and 5b shows the power output.

5. Discussion

The assumption that if the ECM model can accurately represent the cell behaviour, the accuracy of the SOP estimation can be indirectly inferred – see Lu et al. (2018); Hu et al. (2020); Shu et al. (2020) – must be considered with caution. Indeed, the estimation of voltage, SOC and SOH limit the accuracy of the SOP estimation. However, the results shown in Fig. 4 suggest that the accuracy of ECM does not warrant the accuracy of the SOP algorithm.

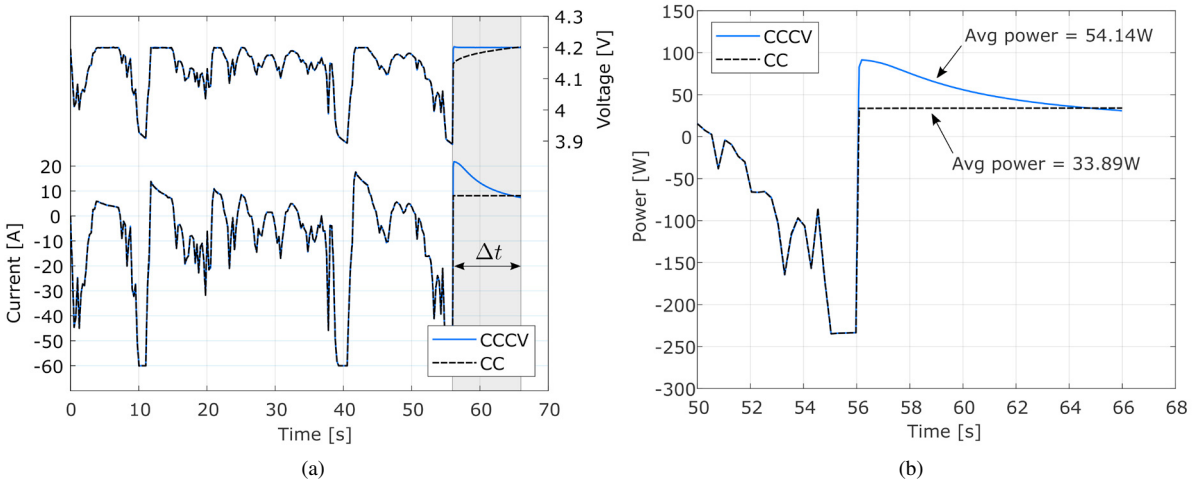

Fig. 5: Experimental comparison between the CCCV and the CV limiting modes. CCCV operates at the voltage limit in every time step. On the other hand, CC only reaches the cell voltage limit at the end of the current pulse. a) Voltage and current profiles. b) Zoom into the power profile. The average power output for a CCCV pulse is 54.14W, whilst for the CC pulse is 33.89W, a difference of 59.75%.

The ECM model used in this research was calibrated precisely for the tested data, arguably over-fitted, on purpose, to achieve low errors. Despite this careful calibration, the error of the SOP estimation is still 10%. This outcome is not unexpected but serves to reinforce the point of the research with empirical evidence. One of the primary reasons for this estimation error is that the model utilised in this paper does not consider the variations in ECM parameters over the future horizon. The inability to account for these parameter changes results in deviations between the estimated SOP and the actual SOP, leading to the observed error (Malysz et al., 2015; Guo and Shen, 2022). More specifically, Equation 10 does not update the ECM parameters over the future horizon, which introduces errors that increase in proportion to the duration of the future horizon. On the other hand, this simplification drastically reduces the computational burden of the algorithm because the voltage at the end of the future horizon is calculated directly with a single time step, whilst the state equations would need many iteration steps to predict the future voltage.

Fig. 5 presented the power output for the CCCV and CC limit modes. As anticipated, the CCCV pulse effectively maintains the voltage limit throughout the entire test duration, whereas the CC mode only reaches the limit towards the end of the future horizon. Specifically, for a 10-second pulse, the average power output for the CCCV mode was 54.14W, whereas for the CC mode, it was 33.89W, indicating a 59.75% higher output for the CCCV mode. The implications of utilising the CC limit mode for SOP estimation are similar to employing overly conservative estimates, resulting in a potential loss of energy retrieval opportunity during braking, as discussed in the literature (Samad et al., 2018; Lin et al., 2019). In consumer automotive applications, striking a balance between battery life and range may be more desirable than pushing the boundaries of regenerative braking. However, for motorsport applications, Figure 5 suggests that exploring these boundaries could be worthwhile.

6. Conclusions

In this study, we investigated the performance of voltage limiting modes for a high-power LCO pouch cell operating at peak power. In addition, an ECM-based SOP estimation algorithm was employed and results were discussed. Our findings shed light on important aspects of validation of SOP algorithms and have implications for future research. Specifically:

1. The accuracy of the ECM does not warrant the accuracy of the SOP estimation algorithm. The many assumptions about how the future states of the cell are computed need careful examination for the intended application. In addition, the influence of these assumptions on the estimation accuracy of the SOP algorithm needs to be assessed through laboratory experiments at peak power.

2. The method proposed by (Guo and Shen, 2022) to iteratively find the limiting current for a given future horizon also works under dynamic load, which suggests the relaxation period between pulses might not be necessary for the cell tested in this research.

3. Our results shows a significant increase in power output when a cell operates in CCCV limit mode, compared to the CC mode. The quantification of this difference highlights the practical implications of CCCV limit mode for regenerative braking, particularly at high SOC. The implications become more pronounced in motorsport applications where there is a constant pursuit of pushing performance boundaries.

Future work will focus on assessing the computational cost of the SOP algorithm employed in this study, particularly in comparison to an ECM that incorporates parameter changes over the future horizon, for example as presented in Xavier et al. (2021). Additionally, the application of CCCV limit mode will be investigated using Model Predictive Control (MPC), an approach that has shown promise in the literature for generating an optimal power profile while considering multiple constraints (Xavier et al., 2020, 2021; Esfandyari et al., 2019).

7. Acknowledgments

We would like to thank OBR Formula Student team, especially Paul Ros Bono and Ananth Shanmugam, for their support with the AVL simulations. We also appreciate Katie Lukow's contributions to the experimental work.

References

Esfandyari, M., Esfahanian, V., Yazdi, M.H., Nehzati, H., Shekoofa, O., 2019. A new approach to consider the influence of aging state on lithium-ion battery state of power estimation for hybrid electric vehicle. Energy 176, 505–520.

Guo, R., Shen, W., 2022. An enhanced multi-constraint state of power estimation algorithm for lithium-ion batteries in electric vehicles. Journal of Energy Storage 50, 104628.

Hu, X., Jiang, H., Feng, F., Liu, B., 2020. An enhanced multi-state estimation hierarchy for advanced lithium-ion battery management. Applied Energy 257, 114019.

Lin, X., Kim, Y., Mohan, S., Siegel, J.B., Stefanopoulou, A.G., 2019. Modeling and estimation for advanced battery management. Annual Review of Control, Robotics, and Autonomous Systems 2, 393–426.

Lu, J., Chen, Z., Yang, Y., Ming, L., 2018. Online estimation of state of power for lithium-ion batteries in electric vehicles using genetic algorithm. Ieee Access 6, 20868–20880.

Lukow, K., 2021. Modular battery pressure fixture. URL: https://github.com/katielukow/MBPF.

Malysz, P., Ye, J., Gu, R., Yang, H., Emadi, A., 2015. Battery state-of-power peak current calculation and verification using an asymmetric parameter equivalent circuit model. IEEE Transactions on Vehicular Technology 65, 4512–4522.

Pei, L., Zhu, C., Wang, T., Lu, R., Chan, C., 2014. Online peak power prediction based on a parameter and state estimator for lithium-ion batteries in electric vehicles. Energy 66, 766–778.

Planden, B., Lukow, K., Collier, G., Morrey, D., 2021. Battery testing consortium. URL: https://github.com/Oxford-Brookes-HVES/BTC.

Plett, G.L., 2004. High-performance battery-pack power estimation using a dynamic cell model. IEEE Transactions on vehicular technology 53, 1586–1593.

Plett, G.L., 2015a. Battery management systems, Volume I: Battery modeling. volume 1. Artech House.

Plett, G.L., 2015b. Battery management systems, Volume II: Equivalent-circuit methods. Artech House.

Samad, N.A., Kim, Y., Siegel, J.B., 2018. On power denials and lost energy opportunities in downsizing battery packs in hybrid electric vehicles. Journal of Energy Storage 16, 187–196.

Shu, X., Li, G., Shen, J., Lei, Z., Chen, Z., Liu, Y., 2020. An adaptive multi-state estimation algorithm for lithium-ion batteries incorporating temperature compensation. Energy 207, 118262.

Xavier, M.A., de Souza, A.K., Plett, G.L., Trimboli, M.S., 2020. A low-cost mpc-based algorithm for battery power limit estimation, in: 2020 American Control Conference (ACC), IEEE. pp. 1161–1166.

Xavier, M.A., de Souza, A.K., Trimboli, M.S., 2021. An lpv-mpc inspired battery sop estimation algorithm using a coupled electro-thermal model, in: 2021 American Control Conference (ACC), IEEE. pp. 4421–4426.

Yang, L., Cai, Y., Yang, Y., Deng, Z., 2020. Supervisory long-term prediction of state of available power for lithium-ion batteries in electric vehicles. Applied Energy 257, 114006.